Quantitative Assessment of Operational Weather Radar Rainfall Estimates over California's Northern Sonoma County Using HMT-West Data

SERGEY Y. MATROSOV

Cooperative Institute for Research in Environmental Sciences, University of Colorado at Boulder, and NOAA/Earth System Research Laboratory, Boulder, Colorado

F. MARTIN RALPH,* PAUL J. NEIMAN, AND ALLEN B. WHITE

NOAA/Earth System Research Laboratory, Boulder, Colorado

(Manuscript received 11 March 2013, in final form 23 August 2013)

ABSTRACT

An evaluation of Weather Surveillance Radar-1988 Doppler (WSR-88D) KMUX and KDAX radar quantitative precipitation estimation (QPE) over a site in California's northern Sonoma County is performed and rain type climatology is presented. This site is next to the flood-prone Russian River basin and, because of the mountainous terrain and remoteness from operational radars, is generally believed to lack adequate coverage. QPE comparisons were conducted for multiyear observations with concurrent classification of rainfall structure using measurements from a gauge and an S-band profiler deployed at the location of interest. The radars were able to detect most of the brightband (BB) rain, which contributed over half of the total precipitation. For this rain type hourly radar-based QPE obtained with a default vertical profile of reflectivity correction provided results with errors of about 50%–60%. The operational radars did not detect precipitation during about 30% of the total rainy hours with mostly shallow nonbrightband (NBB) rain, which, depending on the radar, provided ~(12%–15%) of the total precipitation. The accuracy of radar-based QPE for the detected fraction of NBB rain was rather poor with large negative biases and characteristic errors of around 80%. On some occasions, radars falsely detected precipitation when observing high clouds, which did not precipitate or coexisted with shallow rain (less than 10% of total accumulation). For heavier rain with a significant fraction of BB hourly periods, radar QPE for event totals showed relatively good agreement with gauge data. Cancelation of errors of opposite signs contributed, in part, to such agreement. On average, KDAX-based QPE was biased low compared to KMUX.

1. Introduction

It has been recognized that coverage of the operational S-band (wavelength $\lambda \sim 10$–11 cm) Weather Surveillance Radar-1988 Doppler (WSR-88D) network for quantitative precipitation estimation (QPE) over the coastal western United States has significant limitations and gaps (e.g., Westrick et al. 1999; Maddox et al. 2002; White et al. 2003). In addition to the large distances between WSR-88D sites in many important coastal areas, gaps in operational radar coverage are also often caused by the blockage of radar beams by mountainous terrain at lower radar tilt (elevation) angles (e.g., Young et al. 1999; Miller et al. 2010). This necessitates the use of higher tilt angles, which often causes overshooting of shallow rainfall or sampling higher regions of precipitating clouds, resulting in biased rain accumulation estimates from operational radar data.

A number of flood-prone river basins are in the areas of poor WSR-88D coverage. Hence, it is important to quantify the performance of radar-based QPE there. Despite the existence of rain gauge networks in such areas, the gauge coverage generally is not sufficient. The complexity of the terrain requires relatively highly resolved temporal (5–6 radar scans per hour at a given elevation) and horizontal spatial (1–3 km) radar-derived rainfall information. The limitations of radar QPE are expected to depend on precipitation types varying from

* Current affiliation: Scripps Institution of Oceanography, University of California, San Diego, La Jolla, California.

Corresponding author address: Sergey Y. Matrosov, University of Colorado, CIRES, R/PSD2, 325 Broadway, Boulder, CO 80305. E-mail: sergey.matrosov@noaa.gov

DOI: 10.1175/JHM-D-13-045.1

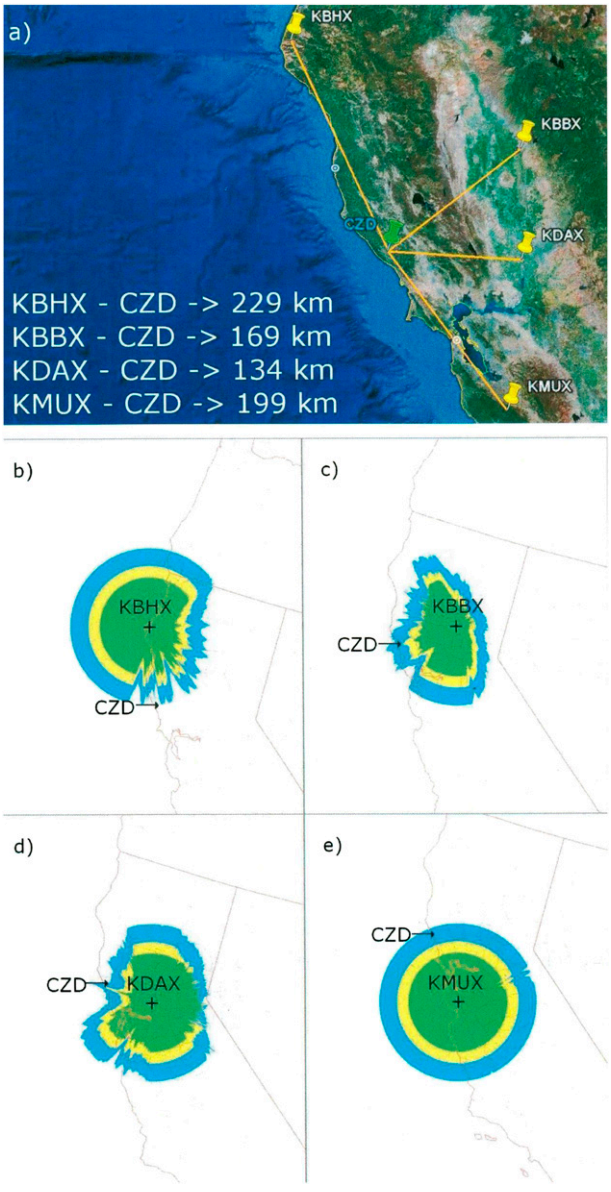

FIG. 1. (a) Locations of different WSR-88D radars relative to the CZD site on the Google Earth image, and maps of the coverage height by the (b) KBHX, (c) KBBX, (d) KDAX, and (e) KMUX radars (from www.ncdc.noaa.gov). Green, yellow, and blue corresponds to coverage at 4000, 6000, and 10 000 ft above radar sites, respectively. Radar site altitudes are 0.73, 0.05, 0.01, and 1.06 km MSL for KBHX, KBBX, KDAX, and KMUX, respectively.

warm rain, which is typically contained in a lower 1–2-km layer where temperatures in the area of interest to this study are generally above freezing even during the winter season, to relatively deep precipitating systems with cloud echo-top heights h_e exceeding 8 km above mean sea level (MSL).

While it is generally believed that the northern Sonoma County lacks adequate WSR-88D coverage (Fig. 1), the extent to which operational radar data can be used in this area is not exactly known. This study aimed to quantify the performance of operational radar-based QPE for different rainfall types using available long-term gauge measurements supported by collocated and simultaneous observations of precipitation regimes. Such measurements are available from a site located near Cazadero (CZD; 38.6107°N, 123.2153°W; 478 m MSL) in California's northern Sonoma County where the National Oceanic and Atmospheric Administration's (NOAA's) Hydrometeorology Testbed-West (HMT; http://hmt.noaa.gov) has operated an S-band vertical profiling precipitation radar (S-PROF; White et al. 2000) and a collocated precipitation gauge (0.01-in. resolution) for several years. The S-PROF provides high-resolution (~60 m) measurements of vertical profiles of equivalent radar reflectivity factor Z_e (hereafter just reflectivity) and vertical Doppler velocity W. These profiles allow classifying precipitation types and their vertical structure. The CZD site is located in an operational radar gap, where WSR-88D coverage is often not available at heights less than ~3 km MSL. It is also in the vicinity of the flood-prone Russian River basin, where improved radar-based QPE can result in better flood forecasting (Ralph et al. 2006; Dettinger et al. 2011).

Factors contributing to QPE errors resulting from retrievals with scanning weather radars include radar-beam overshooting of shallow rain, inferring precipitation at the surface when there are virga instead, using inappropriate relations between reflectivity and rain rate, R, (i.e., Z_e–R relations), and not correcting for vertical profiles of reflectivity (VPR). However, it is rare to be able to diagnose the relative importance of different factors contributing to the overall errors. The availability of long-term S-PROF and rain gauge observations in a climatologically wet coastal mountain location enables such analysis. This study takes advantage of the recent analysis by Ralph et al. (2013) of precipitation events observed during landfalling atmospheric rivers (ARs), which are relatively narrow bands of enhanced water vapor transport associated with extratropical cyclones. These authors showed that AR events observed during only about 1500 h are responsible for 51% of the total CZD 6-yr (fall 2004–summer 2010) precipitation. ARs are also responsible for most flooding in the area of interest (Ralph et al. 2006).

The main objectives of this study were (a) to quantitatively evaluate WSR-88D QPE in a flood-prone mountainous site located in a gap of the operational radar coverage, (b) to stratify the results based on the rain type observed at the ground, and (c) to estimate potential improvements for the WSR-88D QPE based on concurrent data from vertically pointing profilers. Quantitative assessment of QPE results is tied to a broader issue of

how well different rain types are detected by remote operational radars. Another goal of the study was to provide climatological information on duration and intensity of different rain types in this environmentally sensitive area.

2. Datasets and methodology

Overall, during the 6-yr period mentioned above, there were 91 landfalling AR events observed at and near the CZD site using the NOAA HMT instrumentation (Ralph et al. 2013, their Table 1). Strong hydrological events in the Russian River basin are usually associated with such events (Dettinger et al. 2011). Since there were gaps in the deployment of the S-PROF, profiler data at CZD were available for only 58 of the 91 AR events. This study focuses on assessment of WSR-88D-based QPE during these 58 events. An average duration of an AR event, as defined by the integrated water vapor (IWV) exceeding a threshold of 20 mm, which is normally used when defining AR boundaries (e.g., Ralph et al. 2013), was about 16 h.

An example of the S-PROF measurements during one of the landfalling AR is shown in Fig. 2. The duration of this AR event, when IWV exceeded 20 mm, was 9 h between 0100 and 1000 UTC on 22 March 2005. To capture some of the precipitation falling prior to and after the moment when the observed IWV amount crossed the 20-mm threshold, the extended periods, which included 12 h prior to the beginning and 12 h after the end of AR conditions for each event, were considered. Accounting for these extended periods and the average AR duration, there were about 2300 hourly periods for all 58 extended AR events that were analyzed in this study. The overlapping times of extended periods from neighboring (in time) AR events were excluded so no hourly precipitation period was considered more than once.

a. Rainfall type classification based on S-PROF data

As can be seen from Fig. 2, there were different types of rainfall observed on 22 March 2005. The rainfall, for which the main formation mechanism is melting of snow/ice particles, produces a clearly defined reflectivity bright band (BB) located below the melting/freezing level (i.e., the 0°C isotherm). The reflectivity bright band is accompanied by rapid and well-defined transitions in the observed vertical Doppler velocities, which change from values that are typical for ice particles [$\sim$(0.5–1.5) m s^{-1}] to those characteristic of rain drops (5–7 m s^{-1}). Examples of the BB rain marked as rain type 1 are seen in Fig. 2 between 0000 and 0300 UTC and also later during the observation period (e.g., 1800 and 2100 UTC). While BB identifications from scanning radars are possible through a variety of means (e.g., Matrosov et al. 2007; Zhang et al. 2008), the BB correction schemes for QPE are generally effective at closer ranges.

At other times, profiler signatures of rainfall did not exhibit well-defined BB features and corresponding Doppler velocity transitions were relatively more subtle. The examples of such nonbrightband (NBB) rain prevail in Fig. 2 between 0300 and 1800 UTC. NBB rain included such subtypes as shallow warm rain (i.e., rain type 2 in Fig. 2) when echo tops generally were below the freezing level (e.g., between 1300 and 1400 UTC, among other times), NBB high rain with echo tops generally exceeding the environmental freezing level (e.g., between 1400 and 1800 UTC, among other such periods, shown as rain type 3 in Fig. 2), and convective rain (rain type 4) when high reflectivity core plumes extended from the ground to the regions located well above (typically more than 1 km) the environmental freezing level (e.g., around 0600 UTC in Fig. 2). A general NBB rain type, which combined all NBB rain types (i.e., types 2, 3, and 4), was also considered in the analysis. In this study, the rain types were classified in hourly intervals. If different rain types were observed within the same interval, the rain type associated with most profiles within a given hour was prescribed to the entire interval. Different aspects of the objective classification procedure of rain types, differentiating between BB and NBB rain, and estimating BB peak heights based on S-PROF data are described by White et al. (2003). The only subjective part of the classification is identifying convective rain as a distinct category of NBB rain.

In addition to the rain types defined above, precipitation classes considered here included situations when no measurable rain was detected during a given hour at CZD but the radar provided nonzero QPE due to detecting virga or/and high nonprecipitating clouds (rain type 5 in Fig. 2). A separate rain type 6 was also prescribed to hourly periods when the surface gauge provided nonzero estimates from shallow rain while the radar sensed virga and/or high clouds disconnected from the precipitation echo as observed by the S-PROF. For both these types (5 and 6), examples of which are seen in Fig. 2, the scanning radar-based QPE was considered as false.

It has been shown (Kingsmill et al. 2006) that for five distinct synoptic extratropical cyclonic regimes (cold sector, warm front, warm sector, cold front, and cool sector) NBB rain occurred most often during the warm-frontal, warm-sector, and cool-sector regimes. Low level, moisture-laden landfalling flow in the AR environment often results in significant orographic precipitation enhancement in the coastal mountains, including near the CZD site (e.g., Neiman et al. 2005; Ralph et al. 2006).

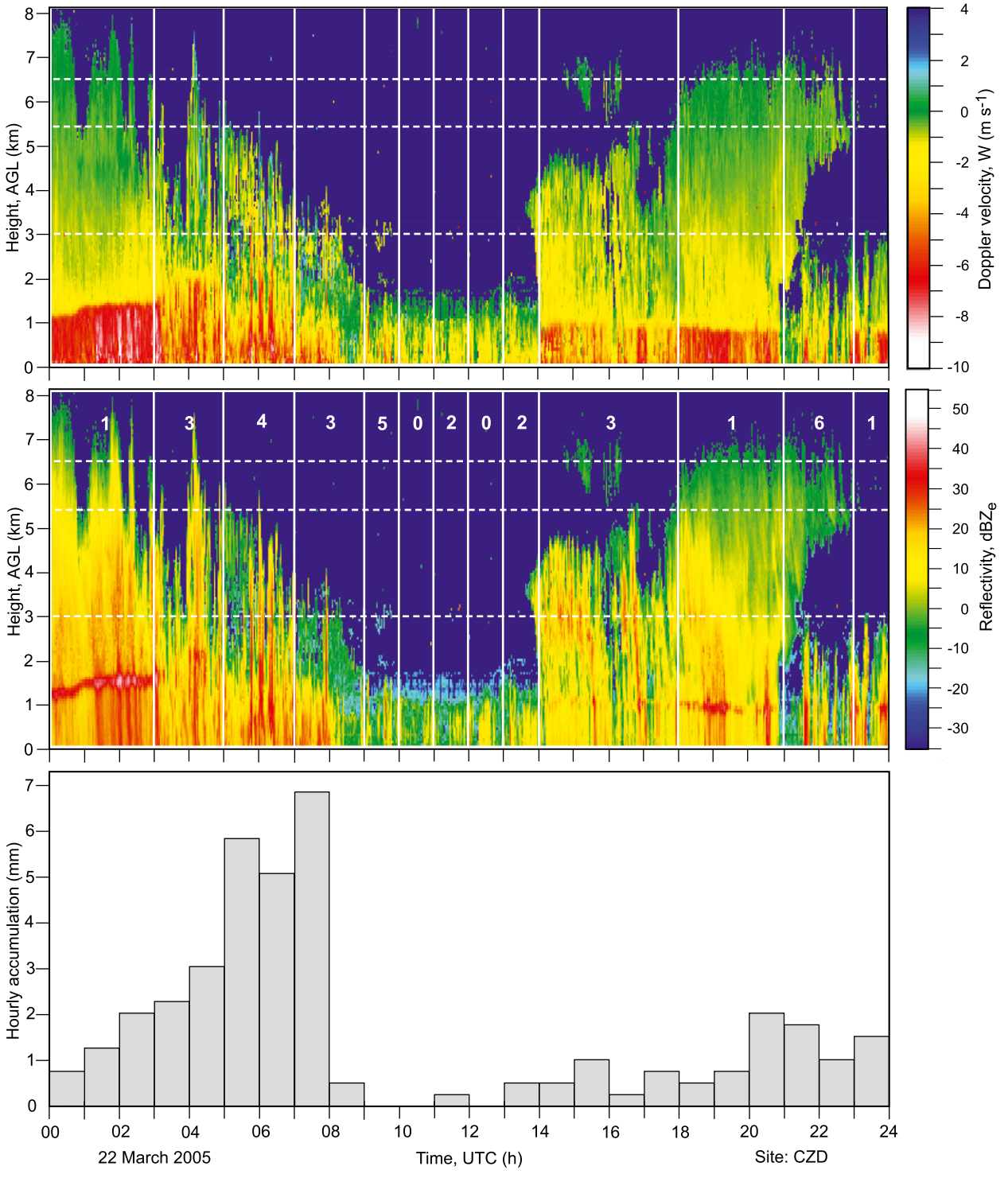

FIG. 2. An example of CZD S-band profiler observations during an AR event observed on 22 Mar 2005: (top) vertical Doppler velocities and (middle) reflectivities. The lower horizontal white line shows expected lower edges of the 0.5° KMUX and 1.5° KDAX beams. The upper and middle horizontal white lines show expected upper edges of the 0.5° KMUX and the 1.5° KDAX beams, respectively. Results of rain classification (for types in Table 1) are shown by white numbers in the middle panel (0 corresponds to no rain from both radar and gauge). (bottom) Hourly accumulations from the CZD gauge.

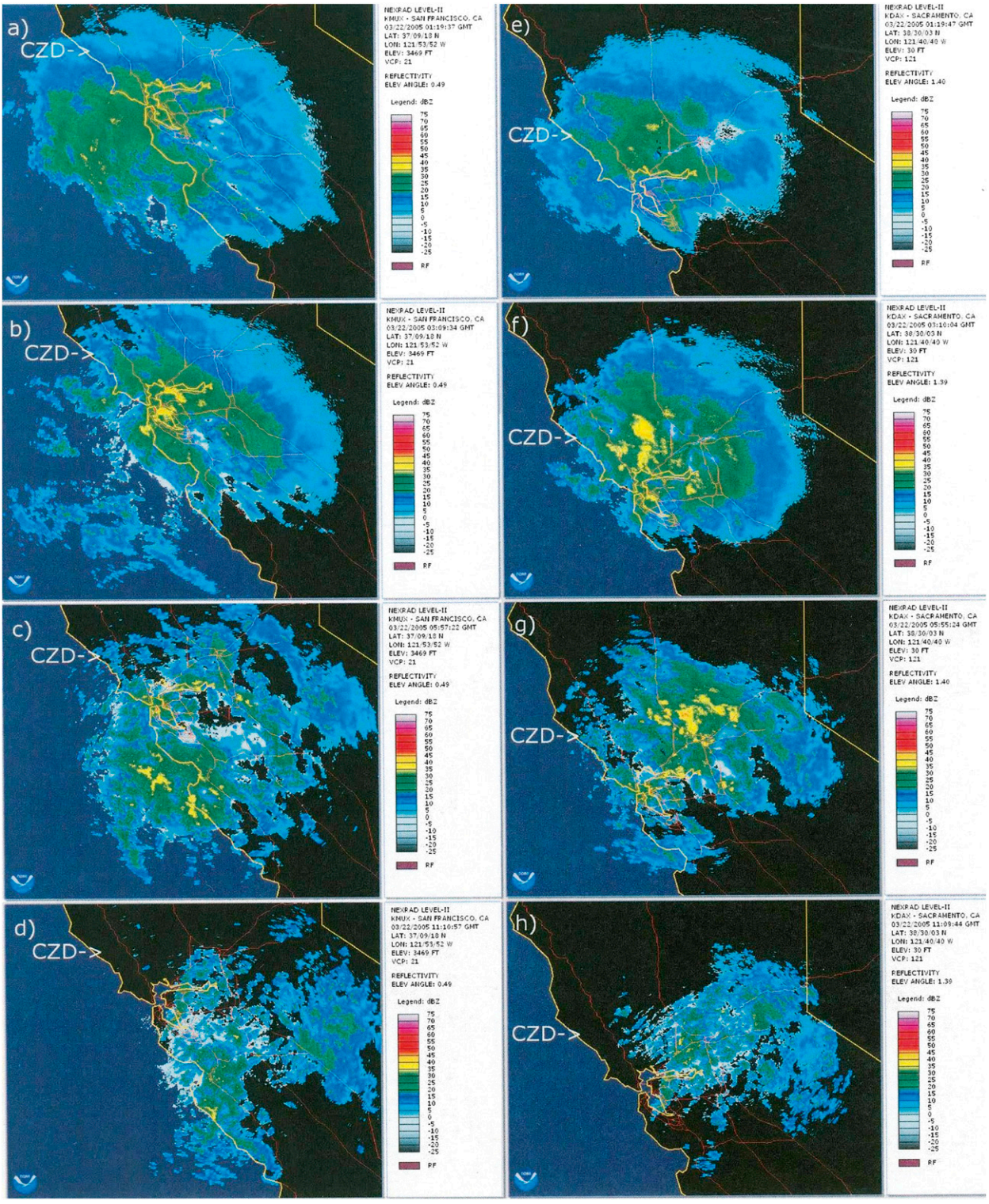

FIG. 3. Examples of (left) KMUX 0.5° tilt and (right) KDAX 1.4° tilt reflectivity measurements during the AR event of 22 Mar 2005 shown in Fig. 1 when precipitation at CZD was classified as (a),(e) BB rain (0119 UTC), (b),(f) NBB high rain (0309 UTC), (c),(g) NBB convective rain (0557 UTC), and (d),(h) NBB warm shallow rain (1111 UTC). Images were generated by the NOAA weather and climate toolkit.

TABLE 1. Results of rain type classification for 58 AR events according the ground data at CZD (except for type 5 precipitation where radar estimates are shown) during cool periods of 2004–10. See detailed explanation in section 2d. Rain type 6 data represent radar QPE and corresponding rain properties were inferred using VPR corrected radar measurements with relation (4) and S-PROF inferred freezing levels. Upper and lower values in data cells correspond to the KMUX and KDAX related data, respectively.

Rain Type No.	1	2	3	4	2 + 3 + 4	5	6	1–6
Rain type	BB rain	NBB rain shallow	NBB rain high	NBB rain convective	NBB rain total	Virga, no CZD rain	Virga with CZD rain	All rain
Total hours	476	479	198	55	732	203	105	1516
	462	417	285	55	757	241	99	1559
Total CZD accumulation (mm)	2301	635	865	357	1856	213 (radar)	224	4382
	2282	496	1041	357	1893	160 (radar)	206	4382
Mean CZD rain rate (mm h^{-1})	4.8	1.3	4.3	6.5	2.5	1.0	2.1	2.9
	4.9	1.2	3.7	6.5	2.5	0.7	2.1	2.8
Mean echo-top AGL	6.7	2.2	4.3	5.0	3.1	N/A	N/A	N/A

b. Selection of WSR-88D radars to use

The WSR-88D radars that are located closest to CZD are in California's Central Valley (i.e., the KDAX radar, located at about 134 km from CZD and the KBBX radar, located at about 169 km from CZD; see Fig. 1). Their views, however, are blocked by the coastal mountains and often the lowest beam tilt (~0.5°) measurements cannot be used. Higher beam tilts and hybrid scans (e.g., O'Bannon 1997) are required to obtain QPE over this terrain. As seen from Figs. 1c and 1d, the valley radars do not provide adequate coverage of offshore regions adjacent to the area of interest.

Various beam blockage fractions necessitating the use of different radar beam tilts can result in spatially discontinuous radar-derived QPE maps (e.g., Zhang et al. 2012). While partial beam blockage algorithms approximately correct for nonsevere beam blockage (e.g., Young et al. 1999), significant uncertainties of such corrections could arise from an assumption of standard radio signal propagation because for any beam direction actual occultation can vary. Although the KMUX WSR-88D radar is located farther from CZD (~199 km) compared to the Central Valley WSR-88D radars, because it is sited at relatively high altitude (~1060 m MSL) it provides an unobstructed view of CZD (and surrounding coastal areas) at the lowest beam tilt of 0.5° (Fig. 1e). The coastal KBHX radar, which is also located high (~740 m MSL) does not provide adequate coverage of the area of interest because of longer distances and considerable blockage (Fig. 1b).

The standard value of the second tilt elevation utilized during most WSR-88D precipitation volume coverage patterns (VCPs) is often 1.5°. At this tilt, center beam directions from the KDAX and KBBX radars to CZD are generally not blocked for normal propagation conditions. In this study, the KMUX 0.5° tilt and the KDAX 1.5° tilt measurements were used for assessments of WSR-88D QPE over the CZD site. It is assumed that, in terms of quality of radar-based QPE, this site is representative of a broader area of Sonoma County, including parts of the flood-prone Russian River basin, and QPE errors obtained for this site are applicable to this broader area. The choice of KDAX over KBBX was dictated by a shorter distance to the CZD site (Fig. 1a).

Because of the sphericity of the earth, the center of a fixed elevation scanning radar beam becomes progressively higher above the ground as range increases. At the same time, the cross-beam resolution becomes coarser with distance. The horizontal white lines in Fig. 2 show the expected levels of the lower and upper edges of the KMUX radar beam over the CZD site. The heights of these levels were calculated using a common approach [e.g., Doviak and Zrnic 1993, their Eq. (2.28)] assuming the 0.95° beamwidth and the 0.5° tilt of the KMUX radar. It can be seen that for a number of hourly time intervals for the example shown in Fig. 2, the radar beam "overshoots" rainfall, which is detected by the S-PROF and measured by the rain gauge (i.e., rain type 2). At the standard 1.5° tilt the lower edge of the KDAX beam above CZD is approximately the same as for KMUX, while the upper edge is at about 5.4 AGL. It should be mentioned, however, that for different analyzed events the exact values of the KDAX tilts, which are nearest to 1.5°, varied from about 1.4° to 1.7°. The actual tilt values were used in the analysis. Note that the lower and upper edges of the 1.5° KBBX radar beam over CZD for normal propagation conditions are about 4.2 and 7.2 km, respectively. For the KBHX radar, these edges over CZD are at about 3.4 and 7.4 km, respectively (for the 0.5° tilt).

c. QPE schemes used with the WSR-88D radar data

Since, as seen from Fig. 2, the radar resolution volume is relatively high above the ground, it is essential to

correct for the vertical profiles of reflectivity in calculating QPE (e.g., Koistinen 1991). VPR corrections are used to predict rain reflectivity near the ground based on radar measurements aloft. Typically, VPR schemes are better suited for stratiform types of precipitation. As such, they assume a decrease in reflectivity with height in snow and ice regions of precipitating systems above the freezing level (FL), a BB reflectivity enhancement due to particle melting, and a nearly constant reflectivity profile in the rain region below the melting layer. Significant uncertainty in VPR reflectivity corrections is associated with BB enhancement assumptions, as this enhancement exhibits significant variability and is progressively smeared as the radar range to observed precipitation increases (e.g., Matrosov 2008).

Examining S-PROF measurements for all 58 observational AR cases showed that freezing levels generally did not exceed 3 km AGL, which indicates that when WSR-88D measurements detect precipitation over the areas near the CZD site, the radar typically samples ice phase hydrometeors except possibly in NBB rain. Because of this fact, VPR uncertainties caused by the BB influence assumptions are avoided when performing QPE retrievals using the radar data. This essentially reduces VPR applications to the assumptions of the reflectivity gradient in the snow/ice regions, dZ_e/dh, and the height of the freezing level h_f. For the purpose of this study it was assumed that $dZ_e/dh = -5\,\mathrm{dB\,km^{-1}}$, which is close to a typical value found during previous HMT studies (Matrosov et al. 2007), who suggested a simple VPR shape (see their Fig. 2) that was also used in the current study. This negative gradient of reflectivity reflects a decrease in ice mass content with height (e.g., Matrosov 1997). In this study, two sets of radar retrievals were performed: one with a common for all observations default value of $h_f = 2.2$ km MSL, which is close to the mean synoptic freezing level at CZD during the cool season (Neiman et al. 2005), and the other with the actual case dependent h_f inferred from the S-PROF estimates of BB heights. As BB maximum reflectivity enhancements are generally located a few hundred meters lower than the 0°C isotherm (e.g., Matrosov 2008), the freezing level heights were assumed to be 0.2 km above the heights of S-PROF BB estimates.

The WSR-88D reflectivity estimates over the CZD site were calculated by interpolation of data obtained at two neighboring azimuthal directions which bracket the direction from a radar site to CZD. Linear interpolation was also used in range to obtain a reflectivity estimate over the CZD site. The data in the super-resolution WSR-88D mode, which has been employed by both radars since mid-2008, were averaged using a three-gate running window to reduce measurement noise.

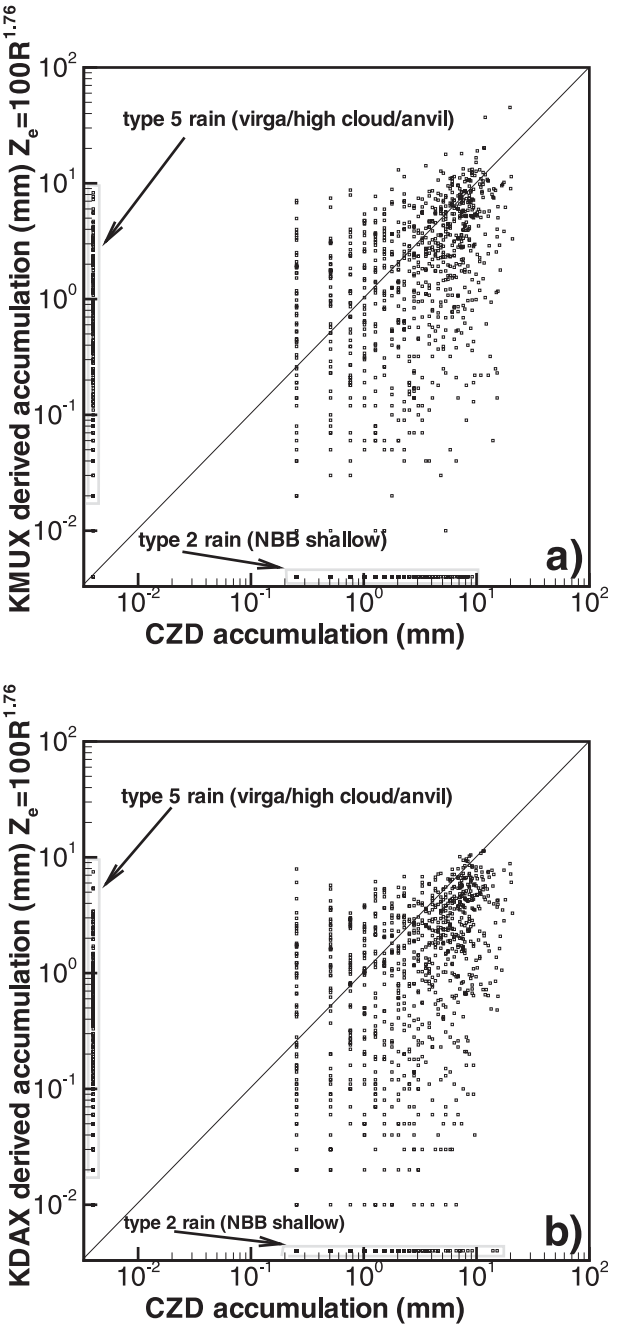

FIG. 4. Scatterplots of all hourly accumulations derived from the CZD gauge and the (a) KMUX and (b) KDAX data obtained with S-PROF inferred freezing level VPR and relation (4).

WSR-88D radars have been recently upgraded to conduct dual-polarization measurements. The dual-polarization data are expected to provide better QPE for regions where radar resolution volumes are filled by rain (i.e., primarily at shorter ranges, where the upper edge of the radar beam is below the freezing level). However, rain rate R retrievals based on conventional radar reflectivity

TABLE 2. Statistical scores characterizing WSR-88D radar based QPE for different Z_e–R relations and VPR freezing levels h_f (km MSL) assumptions as compared to the CZD gauge data for all hourly accumulation measurements for all rain types. Upper and lower values in data cells correspond to the KMUX and KDAX related data, respectively.

	$h_f = 2.2$ km $Z_e = 44R^{1.91}$	$h_f = 2.2$ km $Z_e = 200R^{1.6}$	$h_f = 2.2$ km $Z_e = 75R^{2.0}$	$h_f = 2.2$ km $Z_e = 100R^{1.76}$	S-Prof h_f $Z_e = 44R^{1.91}$	S-Prof h_f $Z_e = 200R^{1.6}$	S-Prof h_f $Z_e = 75R^{2.0}$	S-Prof h_f $Z_e = 100R^{1.76}$
RMB (%)	7.0	−33	−26	−17	−10	−46	−37	−31
	−23	−56	−45	−43	−32	−63	−52	−51
RMSE (mm)	4.7	4.0	3.5	4.1	3.6	3.4	3.2	3.3
	3.2	3.1	3.2	3.2	3.2	3.5	3.3	3.3
NMAE (%)	91	78	76	81	81	73	72	74
	74	75	72	72	72	76	73	73
Correlation, r	0.66	0.61	0.67	0.64	0.70	0.67	0.71	0.69
	0.72	0.69	0.72	0.71	0.72	0.70	0.72	0.71

measurements still are (and will likely remain) an important option for QPE estimates at longer ranges when radar signals are attributable to ice–snow parts of precipitating systems producing rainfall near the ground. Thus, VPR-corrected Z_e–R-based retrievals remain the viable (if not the only) option for WSR-88D-based QPE in the region of interest to this study.

The performance of four different Z_e–R relations, given below, was evaluated in this study:

$$Z_e = 44R^{1.91}, \quad (1)$$

$$Z_e = 200R^{1.6}, \quad (2)$$

$$Z_e = 75R^{2.0}, \quad (3)$$

$$Z_e = 100R^{1.76}. \quad (4)$$

Relation (1) was found by Martner et al. (2008) when they analyzed drop size distribution (DSD) data in NBB rain measured by an impact Joss–Waldvogel disdrometer (JWD) at the CZD site during the cool season of 2004/05. Relation (2) is the standard one used by WSR-88D radars in stratiform rain. It is very close to the average Z_e–R relation for BB rain from Martner et al. (2008), so their BB relation (i.e., $Z_e = 170R^{1.61}$) was not considered in this study separately. In addition to relations (1) and (2), relation (3), which was recommended for cool-season applications in the western United States, and relation (4), found using DSD measurements during HMT-06 field project (Matrosov et al. 2007), were also utilized in this study.

Figure 3 shows examples of KMUX lowest tilt (0.5°) and KDAX 1.4° tilt reflectivity measurements during the event of 22 March 2005 shown in Fig. 2 when rain of different types was detected by the CZD S-PROF. It can be seen that a continuous radar echo is detected during the BB rain (Figs. 3a,e). The gradual echo decrease with range is due to the fact that higher ice regions with lower reflectivity are sensed as range increases. Regions of high NBB rain (i.e., the NBB rain detected by the radars as opposed to shallow NBB rain) are characterized by more discontinuous echoes (Figs. 3b,f). Some cellular echo is observed during convective showers near CZD (Figs. 3c,g). Warm shallow rain over CZD is not detected by both radars at all (Figs. 3d,h). It can also be seen from Fig. 3 that compared to the KDAX radar, the KMUX radar observes more echo offshore, thus providing better coverage of precipitation associated with landfalling ARs.

d. *Intensity and relative duration of different precipitation types observed at CZD*

Totals of 1516 (for KMUX) and 1559 (for KDAX) hourly periods of rain from 58 extended AR events (out of 2300 available) were analyzed in this study. These hours were chosen based on the availability of the CZD rain gauge, the S-PROF and WSR-88D radar observations, and the presence of measurable precipitation in either the rain gauge (>0.01 in.) or radar data (i.e., when the radar reflectivities were above the reported WSR-88D noise level). Several hourly rainy periods during 58 AR events when radars were temporarily not operational were disregarded. Also excluded were periods when neither the gauge nor the operating radar indicated precipitation. Based on S-PROF data analysis, Table 1 presents the results of rain type classification for all hourly periods and shows total hours and accumulations for each rain type. This table also shows mean echo tops h_e estimated from the S-PROF, total rainy hours and accumulations, and the mean CZD rain rate (i.e., the mean gauge hourly accumulation). Summary data for all rain types are shown.

The results are presented separately for all precipitation types defined earlier in section 3a. For type 5, when the radars observed virga or/and high cloud, the radar-derived false accumulations using relation (4) are shown because the corresponding CZD gauge did not

record any precipitation. Periods with erroneous rain detection by radar when high cloud–anvil–virga radar echoes were accompanied by shallow rainfall, which was detached from higher regions of radar returns (i.e., rain type 6), were observed during approximately 7% of all rainy hours for both radars. Such rainfall amounted to about 5% of the total CZD accumulation.

Less than 12 (depending on the radar) rainy hourly intervals classified as BB rain (rain type 1) lacked any accumulations derived from the radar measurements. This was due to low echo-top heights for these intervals (e.g., between 2300 and 2400 UTC in Fig. 2), even though the mean echo-top height for BB rains (i.e., h_e = 6.7 km AGL) was the highest among all rain types. The BB rain produced more than half of the total accumulation measured by the CZD gauge. It is seen from Table 1 that while the total duration of this rain type was about the same as for shallow NBB rain type 2, which went undetected by the radars, BB rain was, on average, about 4 times more intense than shallow NBB rain. The heaviest, on average, was the NBB convective rain (i.e., type 4 rain), although it was observed during less than 4% of all rainy hours.

3. Evaluation of radar-derived hourly rainfall accumulation

It is customary to evaluate the quality of radar-based QPE based on 1-h accumulation values (e.g., Zhang et al. 2012). Evaluation for finer temporal scales is hampered by incremental (i.e., 0.01 in.) estimates of rain gauges and a diminishing number of radar scans at a given tilt as time scales decrease. Scatterplots of WSR-88D derived hourly QPE estimates, a_k, for all hourly intervals versus CZD gauge accumulations, a_c, are depicted in Fig. 4. The results are shown for the QPE retrieval dataset obtained when VPR corrections utilize mean freezing-level heights inferred from the S-PROF data and the Z_e–R relation (4) for calculating rain rates from VPR-corrected estimates of reflectivity near the ground. This relation was obtained using a large set of rain DSDs collected during HMT. Even though the scatterplot data are depicted for relation (4), a detailed statistical evaluation was performed for all relations given by Eqs. (1)–(4).

The incremental character of gauge estimates is manifested in Fig. 4 by the alignment of accumulations along the vertical lines spaced 0.254 mm (0.01 in.) apart. A group of horizontal points that is aligned horizontally near the x axis represents the NBB shallow rain, which is not captured in radar observations. This rain accounts for about 15% (for KMUX) and 12% (for KDAX) of the total observed accumulation. Overall radars completely missed or wrongly identified rainfall, which resulted in

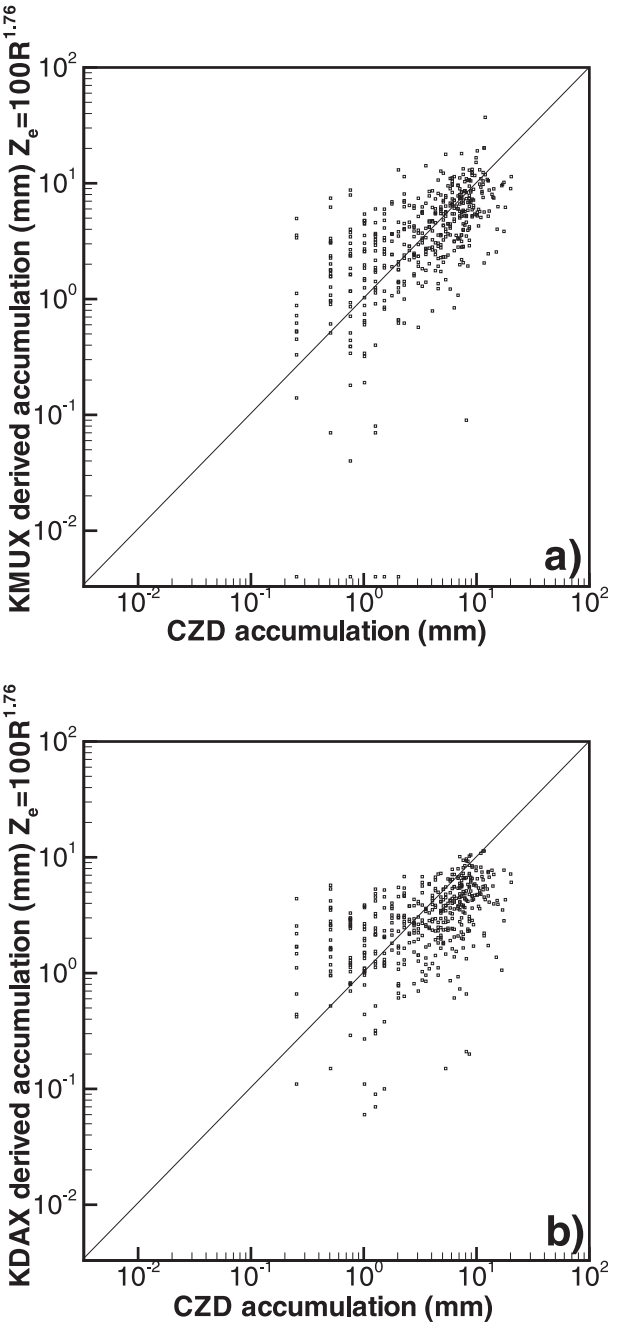

FIG. 5. Scatterplots of hourly accumulations during the BB rain periods (type 1 rain in Table 1) derived from the CZD gauge and the (a) KMUX and (b) KDAX data obtained with S-PROF inferred freezing-level VPR and relation (4).

859 mm (for KMUX) and 702 mm (for KDAX) of gauge accumulation [~(16%–20%) of the total] at CZD (i.e., combined rain types 2 and 6 in Table 1). The group of vertical points near the y axis represents false radar-retrieved rainfall when no accumulation was actually observed at the CZD site. As shown in Table 1, these

TABLE 3. Statistical scores characterizing radar-based hourly QPE for different Z_e–R relations and VPR freezing level h_f, (km MSL) assumptions as compared to the CZD gauge data for hourly accumulations when BB type rain was observed over CZD. Upper and lower values in data cells correspond to the KMUX and KDAX related data, respectively.

	$h_f = 2.2$ km $Z_e = 44R^{1.91}$	$h_f = 2.2$ km $Z_e = 200R^{1.6}$	$h_f = 2.2$ km $Z_e = 75R^{2.0}$	$h_f = 2.2$ km $Z_e = 100R^{1.76}$	S-Prof h_f $Z_e = 44R^{1.91}$	S-Prof h_f $Z_e = 200R^{1.6}$	S-Prof h_f $Z_e = 75R^{2.0}$	S-Prof h_f $Z_e = 100R^{1.76}$
RMB (%)	51	−4	4	17	30	−21	−10	−2
	7	−39	−25	−21	−5	−47	−33	−30
RMSE (mm)	6.5	5.1	4.1	5.4	4.2	3.5	3.2	3.4
	3.5	3.8	3.4	3.5	3.3	4.0	3.6	3.5
NMAE (%)	79	59	55	63	61	51	47	50
	52	54	49	49	49	57	51	51
Correlation, r	0.79	0.73	0.80	0.76	0.83	0.82	0.84	0.85
	0.84	0.82	0.84	0.83	0.83	0.83	0.84	0.85

erroneous radar QPE data amounted to 213 mm (for KMUX) and 160 (for KDAX) of accumulation.

Several statistical estimators were used to quantitatively assess the quality of radar-derived QPE. These estimators were the relative mean bias (RMB),

$$\mathrm{RMB} = (\langle a_k - a_c \rangle / \langle a_c \rangle) 100\%, \tag{5}$$

the root-mean-square error (RMSE),

$$\mathrm{RMSE} = \langle (a_k - a_c)^2 \rangle^{0.5}, \tag{6}$$

and the normalized mean absolute error (NMAE),

$$\mathrm{NMAE} = (\langle |a_k - a_c| \rangle / \langle a_c \rangle) 100\%, \tag{7}$$

where angle brackets mean averaging of hourly accumulations. The statistical estimator scores and corresponding linear correlation coefficients (r) between radar and gauge accumulations are shown in Table 2 for all hourly data points. The radar QPE results were obtained using Z_e–R relations (1)–(4) and the VPR corrections, which utilized the default climatological value for the freezing level height ($h_f = 2.2$ km) and also the mean h_f values inferred from the S-PROF.

As seen from Table 2 the NMAE values of radar QPE based on both freezing-level sources are quite large (70%–90%) and the corresponding RMSE values exceed the mean hourly gauge accumulation (i.e., ~2.9 mm) for all data points. Partial cancellation of errors of different signs from shallow NBB rain and high cloud/virga points (rain types 3 and 6), when either radar or gauge data did not show accumulations, results in small relative mean biases for some Z_e–R relations. Overall, for a given relation and the same FL assumptions, KDAX accumulations are generally lower than those from KMUX. Possible reasons for that will be discussed later.

While Fig. 4 and Table 2 statistics are for all data points including hourly periods of wrong detection (i.e., rain type 6) and those periods when only radar or only gauge reported precipitation (rain types 2 and 5), of special interest are comparisons of rain accumulations when both radar and gauge sensors generally provided data simultaneously from the same precipitating systems. Figure 5 shows scatterplots of radar-derived and gauge hourly accumulations during periods of BB rainfall. The VPR correction with the S-PROF estimates of FL level heights and relation (4) were used to obtain radar data depicted in this figure. As mentioned earlier, BB type rain over CZD was, for the most part, detected by the radars. This rain type is characterized by higher mean intensity (~4.8 mm h^{-1}) than NBB rain (excluding convective periods), and was responsible for about 52% of the total CZD accumulation. The statistical scores characterizing comparisons of WSR-88D QPE and CZD gauge measurements for BB rain are shown in Table 3.

It is evident from comparing Figs. 4 and 5 and Tables 2 and 3 that the agreement between radar and gauge QPE for the BB rain hourly periods is much better than when all hourly data points are considered. For KMUX there is a noticeable improvement when the information on freezing-level heights is inferred from S-PROF data rather than using the default value of $h_f = 2.2$ km MSL. For both radars the Z_e–R relation (4) provides decent results with relatively small biases and NMAE values of around 50%. The correlation coefficients between radar and gauge estimates are quite large (>0.8) using the S-PROF based freezing levels and a bit less when using the default value of $h_f = 2.2$ km. The RMSE values for radar estimates that use S-PROF information are noticeably smaller than the gauge mean hourly accumulation for this rain type (i.e., 4.8 mm).

Scatterplots between radar-derived and gauge measured hourly accumulation data for NBB rain when both sensors detected the same rainfall (i.e., rain types 3 and 4) are depicted in Fig. 6. These data compare significantly worse than for the BB rain type. As shown in Table 4, the

NMAE values for these rain types are on the order of 75%–88%, the corresponding correlation coefficients are relatively low, and the RMSE values often exceed the mean rain intensity observed by the CZD gauge. One factor that contributes to larger disagreements of radar and gauge QPE for NBB rain is that echo-top heights for these rain types are significantly lower than for BB rains (see last row in Table 1), so partial beam filling problems (e.g., Smith et al. 1996) are more acute.

For NBB rain, radar QPE retrievals significantly underestimate accumulations relative to gauge readings as seen by large negative RMB values in Table 4. As expected, the NBB Z_e–R relation (1), which was derived using NBB rain DSDs, performed better than the others, although even for this relation the negative bias is very significant [~(−52%–62%)]. Partial beam filling is one important factor that results in underestimating accumulations from radar measurements in NBB rain. It is evident that the smallest RMB values for the relation $Z_e = 44R^{1.91}$ (compared to RMB values for other relations) for all rain types (see Table 2) to some degree is often due to partial cancellation of positive biases for BB rain and relatively large negative biases for NBB rain.

Unlike for the BB rain, the use of the S-PROF-based FL height information in VPR corrections does not result in appreciable radar-based QPE improvement for NBB rain. This fact is not surprising since the VPR corrections are generally derived for use with stratiform rainfall that exhibits BB features, whereas at least some of the NBB rain is convective in character.

4. Evaluation of radar-derived event total accumulations

In addition to evaluating radar-derived hourly QPE accumulations, it is instructive to analyze uncertainties of event total accumulations from radar measurements, $A_{\text{WSR-88D}}$, using total event amounts from the CZD gauge, A_{CZD}. Figure 7 shows scatterplots of radar event accumulations derived using the Z_e–R relation (4) and the default mean seasonal value of the freezing-level height $h_f = 2.2$ km AGL. Depicted are scatterplots for all 58 AR events (Fig. 7a), as well as different event subsets including the 28 events with a relatively large (>33%) fraction of BB rain profiles (Fig. 7b), the events with total accumulations in excess of 30 mm as estimated from radar measurements (Fig. 7c), and the 21 events with relatively high mean echo-top heights ($h_e > 4.7$ km AGL; Fig. 7d). The statistical characteristics of radar and gauge QPE event total comparisons are shown in Tables 5 and 6 for different Z_e–R relations. The use of the event-dependent values of h_f, as inferred from S-PROF data, generally changes the data scatter by a few percentage points compared to utilizing the mean h_f value. This change, however, is more modest than for individual hourly QPE comparisons, so data corresponding to event total QPE with h_f inferred from S-PROF data are not shown.

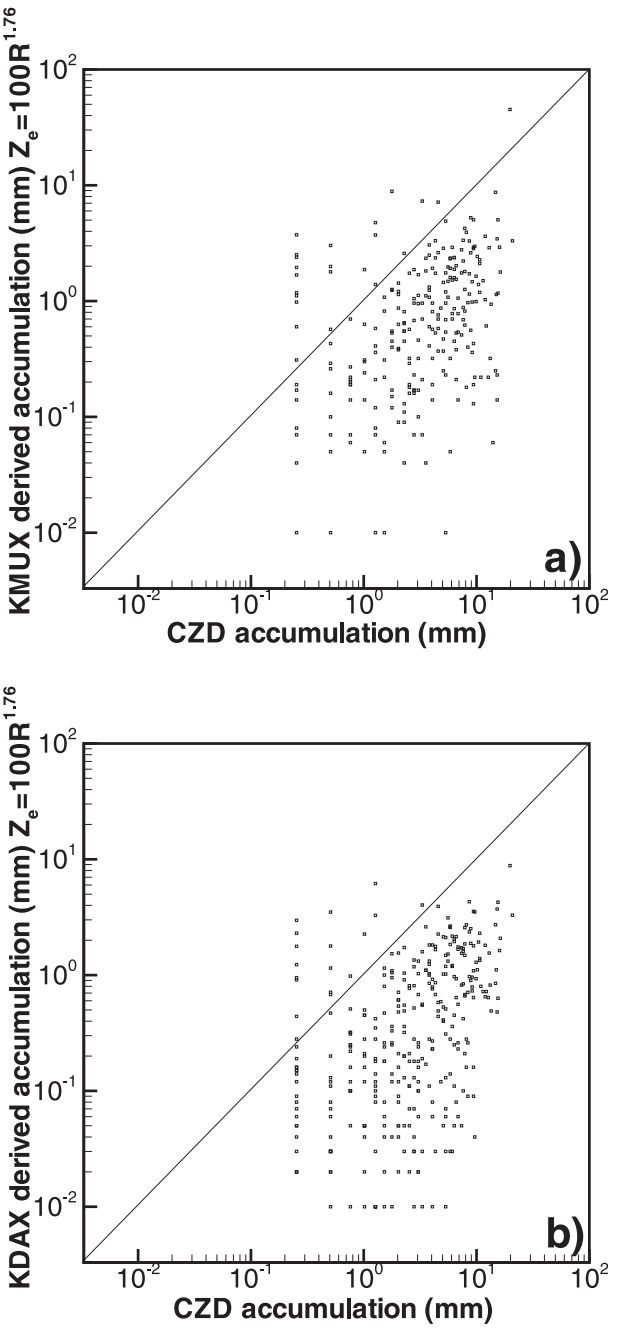

FIG. 6. Scatterplots of hourly accumulations during the NBB rain periods when radar detected rainfall (types 3 and 4 rain in Table 1) derived from the CZD gauge and the (a) KMUX and (b) KDAX data obtained with S-PROF inferred freezing-level VPR and relation (4).

TABLE 4. Statistical scores characterizing radar-based hourly QPE for different Z_e–R relations and VPR freezing-level h_f (in km MSL) assumptions as compared to the CZD gauge data for hourly accumulations for NBB high and convective rain (types 3 and 4), which was simultaneously measured by the radar and the CZD rain gauge. Upper and lower values in data cells correspond to the KMUX and KDAX related data, respectively.

	$h_f = 2.2$ km $Z_e = 44R^{1.91}$	$h_f = 2.2$ km $Z_e = 200R^{1.6}$	$h_f = 2.2$ km $Z_e = 75R^{2.0}$	$h_f = 2.2$ km $Z_e = 100R^{1.76}$	S-Prof h_f $Z_e = 44R^{1.91}$	S-Prof h_f $Z_e = 200R^{1.6}$	S-Prof h_f $Z_e = 75R^{2.0}$	S-Prof h_f $Z_e = 100R^{1.76}$
RMB (%)	−52	−70	−67	−63	−62	−78	−74	−72
	−69	−83	−78	−77	−73	−86	−80	−81
RMSE (mm)	5.7	5.9	5.3	5.7	5.4	5.6	5.3	5.5
	4.4	4.9	4.7	4.7	4.5	5.0	4.8	4.8
NMAE (%)	77	84	79	81	78	87	81	82
	75	86	81	82	79	88	84	85
Correlation, r	0.53	0.44	0.55	0.49	0.54	0.45	0.57	0.51
	0.70	0.66	0.71	0.68	0.71	0.67	0.71	0.68

As seen from Fig. 7a, three AR events were not "sensed" at all by the radars (the corresponding data points are on the x axis). Examining S-PROF data (not shown) indicates that these events were almost entirely associated with shallow warm rain. They produced CZD gauge accumulations of 5.9, 6.2 (these two points almost overlap in Fig. 7a), and 36.1 mm, respectively. There were also a number of AR events (shown inside the dashed-line rectangle in Fig. 7a), for which radar-derived accumulations (while exceeding a few tenths of a millimeter) were significantly smaller than the gauge values observed at CZD. These events, however, as seen from Fig. 7a, were not among the ones that produced heaviest total precipitation amounts.

Twenty-eight AR events with at least a 33% fraction of BB rain type in observed precipitation (Fig. 7b) generally produced more total accumulation (i.e., on average 95.8 mm of CZD totals per event as opposed to 75.6 mm, which is the mean value for all 58 events). The agreement between radar QPE and CZD QPE for these events is noticeably better compared to all event statistics. Corresponding NMAE values for relation (4) are about 35%. This is comparable to the accuracy of storm totals from WSR-88D-based QPE with observations at shorter ranges (e.g., Krajewski et al. 2010) when no VPR corrections for radar measurements were necessary.

Agreement between radar and gauge event total QPE results is better for cases with large observed rainfall amounts. Figure 7c shows the scatterplot for the data when the radar QPE amounts calculated using the relation (4) were in excess of a 30-mm threshold. There were 35 and 31 such events observed by the KMUX and KDAX radars, respectively. According to the gauge, these events produced more than about 80% of the 58 event total rainfall at CZD. Statistical scores in Table 6 show that the data scatter for these events is somewhat larger and correlation coefficients are a bit smaller compared to the subset in Fig. 7b. Corresponding NMAE values, however, exhibit less sensitivity to the choice of the Z_e–R relation.

The event total accumulation estimates from the radar data are, on average, more accurate for precipitating systems that have higher echo tops. This fact is illustrated by Fig. 7d where a subset of 21 AR events was chosen when mean echo-top height was greater than a 4.7-km AGL threshold. This subset provided about half of the total CZD accumulation. The 4.7-km AGL threshold approximately corresponds to the center of the lowest tilt KMUX beam over CZD, which means that the partial beam filling effects negatively affecting reflectivity measurements are not very severe. For full beam filling, WSR-88D minimum detectable reflectivity is about −5 dBZ at 200 km (D. Burgess 2012, personal communication), which approximately corresponds to values near echo fringes in Fig. 2. It should be mentioned, however, that the reported CZD S-PROF reflectivity values might be somewhat biased because of drifts in receiver–transmitter properties. The absolute calibration uncertainties of the S-PROF, however, do not affect rainfall type classification results. Statistical score characteristics (Table 6) for the 21 events with high echo tops are rather similar to those for the subset of events with higher fractions of BB rain.

The subsets of AR events shown in Figs. 7b–d partially overlap, as precipitating systems with larger fraction of BB rain type generally have higher echo tops and tend to produce larger amounts of precipitation. While choosing an event with certain BB rain fractions or echo-top height thresholds requires simultaneous S-PROF measurements, a choice based on radar totals (i.e., Fig. 7c) is based solely on WSR-88D radar data. This indicates that radar-based estimates of the event accumulations could be on average satisfactory if those estimates produce larger amounts (e.g., greater than 30 mm). A caveat here is that one factor contributing to decent agreement of total

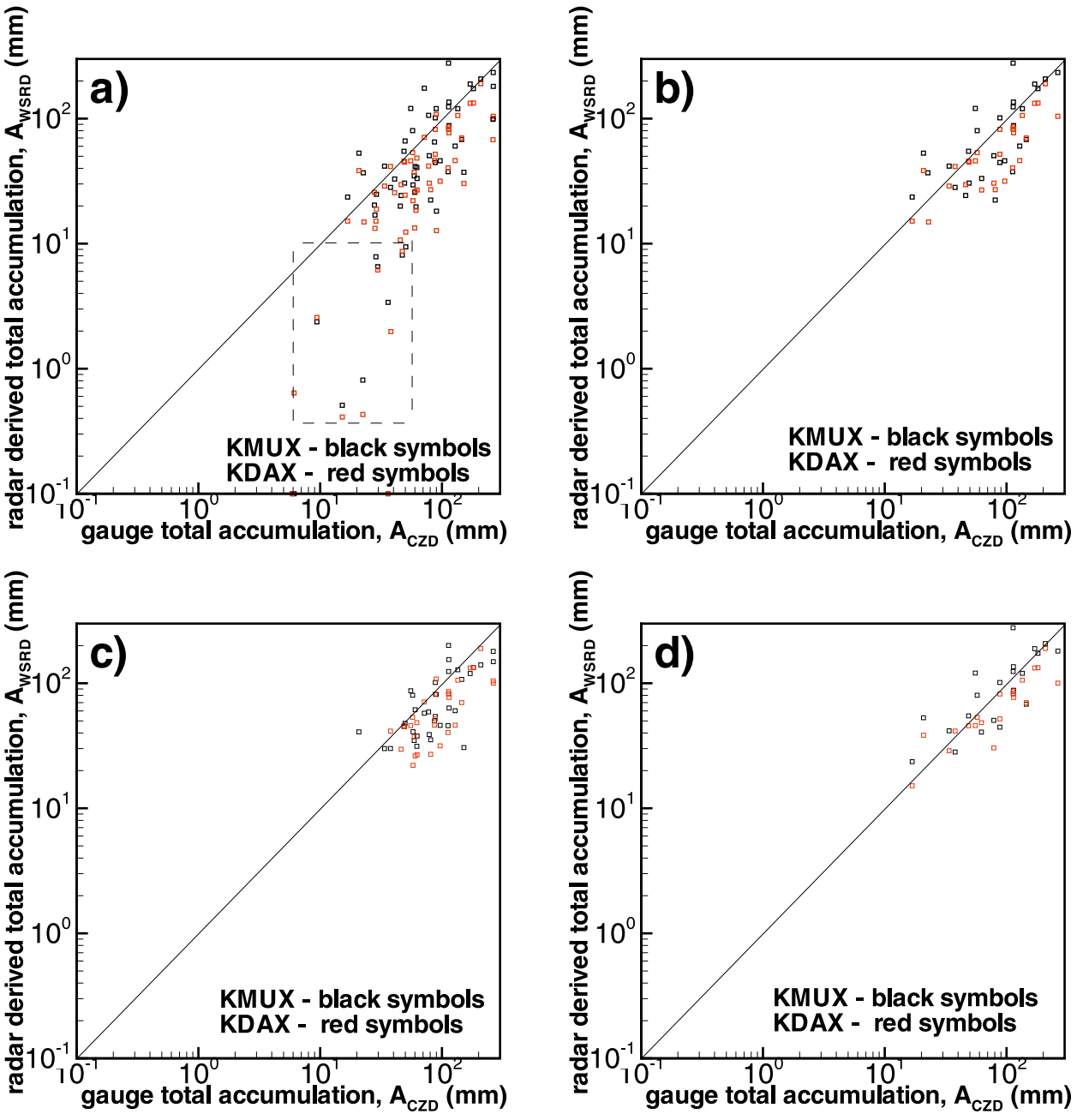

FIG. 7. Scatterplots of event-total radar-derived rain accumulations using h_f = 2.2 km and relation (4) vs gauge data for (a) all 58 AR events, (b) events when BB rain fraction was >33%, (c) events when radar data QPE was >30 mm, and (d) events with mean cloud-top heights > 4.7 km AGL. Data within a dashed line rectangle in Fig. 7a represent events for which the KMUX QPE significantly underestimated gauge data.

accumulations for some events is partial cancellation of underestimating (overestimating) accumulation periods when the radar does not detect (falsely detects) precipitation (i.e., type 2 vs type 5 precipitation in Table 1) and periods of detached cloud and precipitation echoes (i.e., type 6 precipitation in Table 1) when radar estimates are erroneous.

It can be seen from Tables 5 and 6 that KDAX-derived event total accumulations are on average smaller than those from KMUX. Figure 8a, where such accumulations derived from these two radars are compared using the Z_e–R relation (4), illustrates this fact. The mean bias of KDAX totals relative to the KMUX totals is about −25%. Correlation between KMUX and KDAX QPE

TABLE 5. Statistical scores characterizing radar-based total event accumulations for different Z_e–R relations for all 58 AR events and subset of 28 events with BB rain fraction (BB_f) greater than 33%. Upper and lower values in data cells correspond to the KMUX and KDAX related data, respectively.

h_f, is above MSL	$h_f = 2.2$ km $Z_e = 44R^{1.91}$ all events	$h_f = 2.2$ km $Z_e = 200R^{1.6}$ all events	$h_f = 2.2$ km $Z_e = 75R^{2.0}$ all events	$h_f = 2.2$ km $Z_e = 100R^{1.76}$ all events	$h_f = 2.2$ km $Z_e = 44R^{1.91}$ ($BB_f > 33\%$)	$h_f = 2.2$ m $Z_e = 200R^{1.6}$ ($BB_f > 33\%$)	$h_f = 2.2$ km $Z_e = 75\ R^{2.0}$ ($BB_f > 33\%$)	$h_f = 2.2$ km $Z_e = 100R^{1.76}$ ($BB_f > 33\%$)
Number of events	58	58	58	58	28	28	28	28
Mean A_{CZD} (mm)	75.6	75.6	75.6	75.6	95.8	95.8	95.8	95.8
Mean $A_{WSR\text{-}88D}$	81.2	50.6	56.0	62.5	117.2	71.7	81.2	89.5
(mm)	58.6	32.9	41.4	43.1	85.7	47.8	60.6	62.8
RMB (%)	7	−33	−26	−17	22	−25	−15	−7
	−22	−56	−45	−43	−11	−50	−36	−34
RMSE (mm)	51.2	48.1	41.3	44.4	60.5	50.8	42.4	47.4
	38.3	57.2	49.0	47.7	35.6	61.5	49.8	48.2
NMAE (%)	48	49	41	43	47	41	34	35
	36	57	47	45	26	51	38	36
Correlation, r	0.78	0.73	0.79	0.76	0.76	0.71	0.77	0.74
	0.81	0.79	0.81	0.80	0.82	0.80	0.82	0.81

results, however, is very high with the correlation coefficient being approximately 0.95. The underestimation of rainfall from KDAX relative to KMUX is also present for hourly accumulations as shown in Fig. 8b. The correlation coefficient between radar hourly accumulations is approximately 0.8. One plausible explanation of the KDAX–KMUX bias is differences in calibration and/or in losses due to attenuation along the propagation paths.

Although calibrations are performed using common procedures, reflectivity offsets between neighboring WSR-88D radars are often present (e.g., Gourley et al. 2003). An independent recent study based on spring 2012 data using Davis, California, HMT site data (D. Kingsmill 2012, personal communication) indicated that while the KMUX reflectivities were in good agreement with disdrometer-based estimates, KDAX reflectivities were biased low relative to KMUX by about 3 dB. A detailed investigation of relative miscalibration between KMUX and KDAX radars over a multiyear period is, however, beyond the scope of the current study. With a possibility of such miscalibration, it should be mentioned that generally smaller biases (in the absolute sense) of KDAX QPE obtained with the use of the Z_e–R relation (1) could be just a consequence of the fact that this relation compared to other considered here relations generally produces higher rain rates for the same reflectivities.

TABLE 6. Statistical scores characterizing radar-based total event accumulations for different Z_e–R relations for a subset of AR events with total radar accumulations greater than 30 mm [using relation (4)] and a subset of 21 events with mean echo-top heights $h_e > 4.7$ km AGL. Upper and lower values in data cells correspond to the KMUX and KDAX related data, respectively.

h_f, is above MSL	$h_f = 2.2$ km $Z_e = 44R^{1.91}$ $A_{WSR\text{-}88D} >$ 30 mm	$h_f = 2.2$ km $Z_e = 200R^{1.6}$ $A_{WSR\text{-}88D} >$ 30 mm	$h_f = 2.2$ km $Z_e = 75R^{2.0}$ $A_{WSR\text{-}88D} >$ 30 mm	$h_f = 2.2$ km $Z_e = 100R^{1.76}$ $A_{WSR\text{-}88D} >$ 30 mm	$h_f = 2.2$ km $Z_e = 44R^{1.91}$ $h_e > 4.7$ km	$h_f = 2.2$ km $Z_e = 200R^{1.6}$ $h_e > 4.7$ km	$h_f = 2.2$ km $Z_e = 75R^{2.0}$ $h_e > 4.7$ km	$h_f = 2.2$ km $Z_e = 100R^{1.76}$ $h_e > 4.7$ km
Number of events	35	35	35	35	21	21	21	21
	31	31	31	31				
Mean A_{CZD} (mm)	102.1	102.1	102.1	102.1	102.2	102.2	102.2	102.2
	105.3	105.3	105.3	105.3				
Mean $A_{WSR\text{-}88D}$	121.6	76.5	83.6	94.0	136.9	84.5	94.5	104.9
(mm)	91.3	51.6	64.3	67.4	99.6	56.0	70.2	73.3
RMB (%)	19	−25	−18	−8	34	−17	−8	3
	−13	−51	−39	−36	−3	−45	−31	−28
RMSE (mm)	62.8	57.0	48.2	52.7	65.8	52.0	43.4	49.4
	42.8	68.4	57.0	55.1	34.8	61.4	49.7	46.7
NMAE (%)	46	43	36	38	46	37	30	31
	27	51	40	37	21	46	33	30
Correlation, r	0.68	0.62	0.70	0.66	0.74	0.68	0.75	0.72
	0.75	0.72	0.75	0.73	0.84	0.83	0.84	0.83

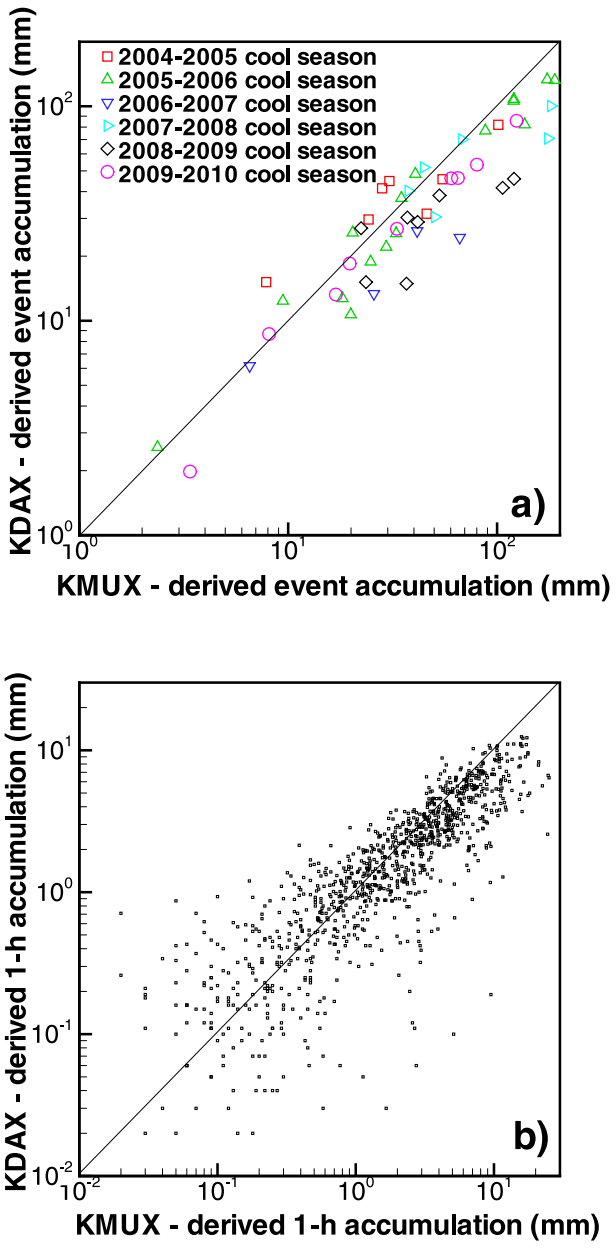

FIG. 8. Comparisons of KMUX and KDAX-derived (a) event total and (b) hourly accumulations.

5. Discussion and conclusions

Evaluation of the KMUX and KDAX radar-derived QPE over the NOAA HMT Cazadero (CZD) site in northern Sonoma County, located in an area of relatively poor WSR-88D network coverage, showed that the uncertainty of radar estimates strongly depends on the type of rainfall. Measurements from the S-PROF deployed at CZD were used to classify rainfall in several types, such as brightband (BB) and nonbrightband (NBB) rain (including convective rain and shallow warm rain), and to infer echo-top and BB heights. The dataset was composed of measurements taken simultaneously by the S-PROF and WSR-88D radars during 58 atmospheric river (AR) events observed over the cool-season periods of 2005–10. The radar QPE procedures included the VPR corrections. The heights of radar resolution volumes were such that they rarely intersected the bright band. Figure 9 schematically illustrates rain classifications, provides information about contributions of different rain types to the total accumulations, and shows absolute biases of radar hourly QPE obtained using the S-PROF information on freezing-level heights utilized in the VPR correction. These biases were calculated as $\Sigma(a_k - a_c)$, where the summation was performed over all hourly periods within a given rain type.

Overall more than 1500 hourly periods with measureable rain from gauge and/or radar data were analyzed. During these periods 4382 mm of rain were measured at the ground. Radars and the gauge observed the same precipitating systems during half of all rainy periods (including BB and NBB high and convective rain), during which more than about 80% of the total rainfall fell. Because of the high altitude of the radar resolution volumes above the ground for the tilts used (i.e., ~0.5° and ~1.5° for KMUX and KDAX, respectively), the radars were not able to detect shallow NBB rain, which was largely warm rain. The number of hours of missed shallow NBB rain by the KDAX radar was about 15% less than for the KMUX radar. The radars were able to detect most of the BB rain, which produced about 2300 mm of accumulation over approximately 470 h of observations. Since they were sensing high-altitude ice clouds or/and anvils, the radars falsely detected 112–299 mm (depending on the radar and the Z_e–R relation choice) of precipitation when no rain was recorded on the ground. During approximately 100 hourly periods the radars detected rain, but for the wrong reason. Specifically, radar sensed high clouds and/or virga instead of shallow rain, which produced slightly over 200 mm of precipitation at the ground.

If all rainy periods are considered, the radars, on average, underestimated 1-h accumulations at the ground with mean NMAE values on the order of 70%–90% and relative mean biases varying from small positive values to as low as about −60% depending on the choice of the Z_e–R relation. These bias estimates, however, were influenced by the periods of shallow rain, which was not observed by the radars, and periods of radar false rain detections. The negative biases for KDAX QPE were larger (in the absolute sense) compared to KMUX QPE. Differences in the radar calibrations and/or losses might be responsible (at least in part) for this effect.

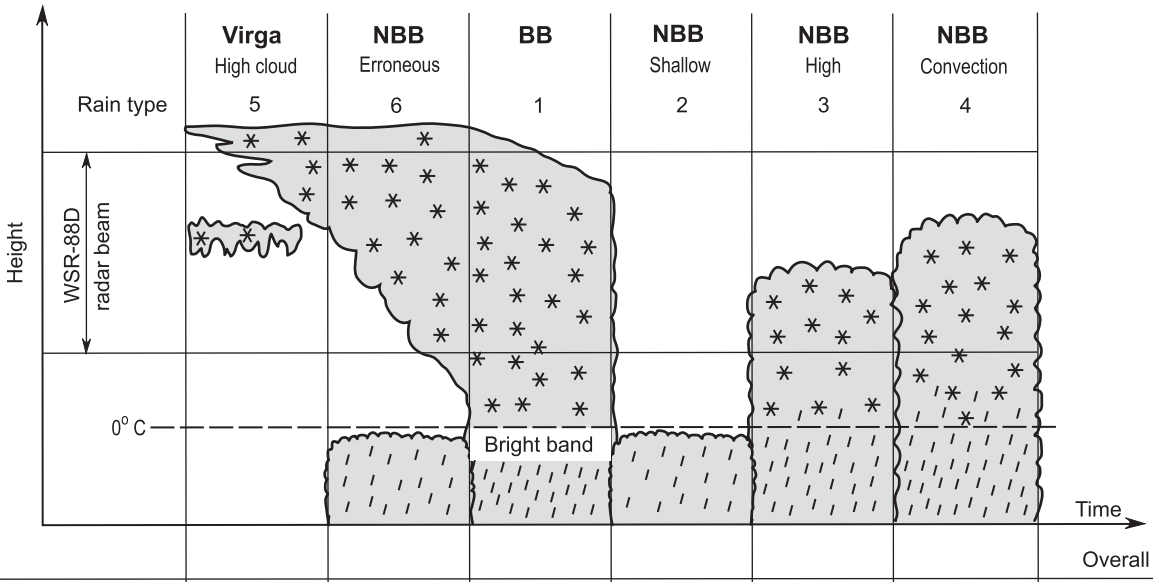

							Overall
KMUX							
Total CZD accumulation	0 mm	224 mm	2301 mm	635 mm	865 mm	357 mm	4382 mm
Absolute bias, Z_e-R (1)	299 mm	-28 mm	685 mm	-635 mm	-601 mm	-151 mm	-431 mm
Absolute bias, Z_e-R (2)	159 mm	-117 mm	-487 mm	-635 mm	-725 mm	-229 mm	-2033 mm
Absolute bias, Z_e-R (3)	214 mm	-84 mm	-233 mm	-635 mm	-676 mm	-218 mm	-1630 mm
Absolute bias, Z_e-R (4)	217 mm	-79 mm	-31 mm	-635 mm	-672 mm	-200 mm	-1399 mm
KDAX							
Total CZD accumulation	0 mm	206 mm	2282 mm	496 mm	1041 mm	357 mm	4382 mm
Absolute bias, Z_e-R (1)	233 mm	-27 mm	-122 mm	-492 mm	-792 mm	-224 mm	-1424 mm
Absolute bias, Z_e-R (2)	112 mm	-113 mm	-1079 mm	-492 mm	-908 mm	-284 mm	-2764 mm
Absolute bias, Z_e-R (3)	170 mm	-77 mm	-766 mm	-492 mm	-853 mm	-263 mm	-2281 mm
Absolute bias, Z_e-R (4)	160 mm	-78 mm	-699 mm	-492 mm	-862 mm	-260 mm	-2231 mm

FIG. 9. Schematic presentation of different rain types and absolute biases of radar hourly rainfall accumulation estimates for these rain types.

For BB rain only, mean radar QPE NMAE values were around 50%–60%, with smaller relative biases [<30% in the absolute sense when the Z_e–R relation (4) was used]. The use of the S-PROF-derived freezing level heights, instead of the mean default value in the VPR scheme, reduced radar QPE errors and biases by several percentage points. The presented results suggest that in spite of the remoteness of the WSR-88D radars, their VPR-corrected QPE could be generally satisfactory in BB rain, which is the rain type contributing the most accumulation. For NBB rain, which was observed simultaneously by the radars and CZD rain gauge, negative biases for the hourly data were approximately −50% to −80%. A factor contributing to poor agreement between the radar data and gauge observations is low mean radar echo heights for this rain type. VPR corrections work better for deep stratiform rainfall and are not optimized for NBB rain.

Comparisons of radar QPE with gauge data for event total accumulations indicated relatively good agreement for events that had a significant fraction of BB rain and higher echo-top heights. Such events generally produced heavier precipitation. For subsets of events with mean echo-top heights in excess of 4.7 km AGL and the BB rain fraction exceeding 33%, mean radar-derived total accumulation errors were relatively low [~(30%–40%)] when the Z_e–R relations (3) or (4) were used. High correlation was observed between KMUX and KDAX QPE results.

A relatively simple VPR correction scheme used in this study assumed a linear (in the decibel scale) decrease of reflectivity with height above the freezing level with

a gradient dZ_e/dh of $-5\,\mathrm{dB\,km^{-1}}$ and a constant reflectivity profile in the rain layer. While this VPR provided a generally decent agreement between radar QPE and gauge data for BB rains, the reflectivity gradients can vary. It appears that the VPR utilized here may reflect some mean conditions and seems to be appropriate for observed BB rains.

The results of this study indicate that the use of profilers such as the S-PROF for identifying rain type, echo-top heights, and the VPR vertical structure operationally at different locations is one way to improve radar-based QPE in the area of interest. Accounting for FL heights based on profiler data improves QPE by few percentage points on average compared to the default VPR. Potential improvements in VPR shapes and accounting for partial beam filling effects for detected rain with lower echo tops based on profiler data will most likely further improve QPE, especially for NBB rainfall. Deploying profilers in environmentally sensitive areas is one important activity of the NOAA HMT Program.

The total accumulations for the events when the radar-derived estimates exceeded 30 mm (and thus flooding hazards were more likely) compared favorably with gauge data. An advantage for identifying such events is that no auxiliary information on rain types and echo-top heights from the profiler measurements is necessary and only WSR-88D information is used in identifying such events (even though accounting for the profiler information still improves the general improvement with ground data). These events usually contained larger fractions of BB rain. One caveat for event-total QPE comparisons is that partial cancellation of errors from no radar rain periods (e.g., rain type 2) and periods when the radar detects virga/high clouds can occur when both such periods are observed within the same event.

The KMUX radar has an unobstructed view of the entire area of interest at the lowest tilt. Observations with the KDAX radar over some regions in the area might have differing occultation at the 1.5° tilt even though the direction along the KDAX-CZD line is largely unblocked at this tilt under the assumption of normal propagation. It will be instructive in the future to assess if radar QPE can reproduce the spatial variability of rainfall in the larger area of interest.

The challenge of observing precipitation in the Russian River basin reflects conditions across much of the western United States where weather service radars alone cannot adequately detect orographic precipitation, which is often relatively shallow. The converse problem, when high cloud/virga is seen by a distant radar and misrepresented as precipitation at the ground, is also an issue (e.g., White et al. 2003; Kingsmill et al. 2006). This study provides an evaluation of these issues over multiple cool seasons with profiler data used to quantify the errors separately. The findings will aid in the identification of underobserved regions across the western United States, and in consideration of alternative methods for filling the gaps. The lessons learned from this study are relevant to many basins from California to Washington State (e.g., the Eel River in California, Nehalem and Smith Rivers in Oregon, and Chehalis River in Washington). Extreme precipitation events in these basins are also associated with AR conditions (Dettinger et al. 2011; Neiman et al. 2011).

Acknowledgments. This study was funded by the NOAA HMT project.

REFERENCES

Dettinger, M. D., F. M. Ralph, T. Das, P. J. Neiman, and D. Cayan, 2011: Atmospheric rivers, floods, and the water resources of California. *Water,* **3,** 455–478, doi:10.3390/w3020445.

Doviak, R. J., and D. S. Zrnic, 1993: *Doppler Radar and Weather Observations.* Academic Press, 562 pp.

Gourley, J. J., B. Kaney, and R. A. Maddox, 2003: Evaluating the calibration of radars: A software approach. *Extended Abstracts, 31st Int. Conf. on Radar Meteorology,* Seattle, WA, Amer. Meteor. Soc., P3C.1. [Available online at https://ams.confex.com/ams/32BC31R5C/techprogram/paper_64171.htm.]

Kingsmill, D. E., P. J. Neiman, F. M. Ralph, and A. B. White, 2006: Synoptic and topographic variability of Northern California precipitation characteristics in landfalling winter storms observed during CALJET. *Mon. Wea. Rev.,* **134,** 2072–2094, doi:10.1175/MWR3166.1.

Koistinen, J., 1991: Operational correction of radar rainfall errors due to the vertical reflectivity profile. Preprints, *25th Int. Conf. on Radar Meteorology,* Paris, France, Amer. Meteor. Soc., 91–94.

Krajewski, W. F., G. Villarni, and J. A. Smith, 2010: Radar-rainfall uncertainties: Where are we after thirty years of effort? *Bull. Amer. Meteor. Soc.,* **91,** 87–94, doi:10.1175/2009BAMS2747.1.

Maddox, R., J. Zhang, J. J. Gourley, and K. Howard, 2002: Weather radar coverage over contiguous United States. *Wea. Forecasting,* **17,** 927–934, doi:10.1175/1520-0434(2002)017<0927:WRCOTC>2.0.CO;2.

Martner, B. E., S. E. Yuter, A. B. White, S. Y. Matrosov, D. E. Kingsmill, and F. M. Ralph, 2008: Raindrop size distributions and rain characteristics in California coastal rainfall for periods with and without a radar bright band. *J. Hydrometeor.,* **9,** 408–425, doi:10.1175/2007JHM924.1.

Matrosov, S. Y., 1997: Variability of microphysical parameters in high-altitude ice clouds: Results of the remote sensing technique. *J. Appl. Meteor.,* **36,** 633–648, doi:10.1175/1520-0450-36.6.633.

——, 2008: Assessment of radar signal attenuation caused by the melting hydrometeor layer. *IEEE Trans. Geosci. Remote Sens.,* **46,** 1039–1047, doi:10.1109/TGRS.2008.915757.

——, K. A. Clark, and D. E. Kingsmill, 2007: A polarimetric radar approach to identify rain, melting-layer, and snow regions for applying corrections to vertical profiles of reflectivity. *J. Appl. Meteor. Climatol.,* **46,** 154–166, doi:10.1175/JAM2508.1.

Miller, D. A., D. Kitzmiller, S. Wu, and R. Setzenfand, 2010: Radar precipitation estimates in mountainous regions: Corrections

for partial beam blockage and general coverage limitations. *Extended Abstracts, 24th Conf. on Hydrology,* St. Louis, MO, Amer. Meteor. Soc., 7.2. [Available online at https://ams.confex.com/ams/90annual/techprogram/paper_163622.htm.]

Neiman, P. J., G. A. Wick, F. M. Ralph, B. E. Martner, A. B. White, and D. E. Kingsmill, 2005: Wintertime nonbrightband rain in California and Oregon during CALJET and PACJET: Geographic, interannual, and synoptic variability. *Mon. Wea. Rev.,* **133,** 1199–1223, doi:10.1175/MWR2919.1.

——, L. J. Schick, F. M. Ralph, M. Hughes, and G. A. Wick, 2011: Flooding in western Washington: The connection to atmospheric rivers. *J. Hydrometeor.,* **12,** 1337–1358, doi:10.1175/2011JHM1358.1.

O'Bannon, T., 1997: Using a terrain-based hybrid scan to improve WSR-88D precipitation estimates. Preprints, *28th Int. Conf. on Radar Meteorology,* Austin, TX, Amer. Meteor. Soc., 506–507.

Ralph, F. M., P. J. Neiman, G. A. Wick, S. I. Gutman, M. D. Dettinger, D. R. Cayan, and A. B. White, 2006: Flooding on California's Russian River: Role of atmospheric rivers. *Geophys. Res. Lett.,* **33,** L13801, doi:10.1029/2006GL026689.

——, T. Coleman, P. Neiman, R. Zamora, and M. Dettinger, 2013: Observed impacts of duration and seasonality of atmospheric-river landfalls on soil moisture and runoff in coastal northern California. *J. Hydrometeor.,* **14,** 443–459, doi:10.1175/JHM-D-12-076.1.

Smith, J. A., D.-J. Seo, M. Baeck, and M. Hudlow, 1996: An intercomparison study of NEXRAD precipitation estimates. *Water Resour. Res.,* **32,** 2035–2045, doi:10.1029/96WR00270.

Westrick, K. J., C. F. Mass, and B. A. Colle, 1999: The limitations of the WSR-88D radar network for quantitative precipitation measurement over the coastal western United States. *Bull. Amer. Meteor. Soc.,* **80,** 2289–2298, doi:10.1175/1520-0477(1999)080<2289:TLOTWR>2.0.CO;2.

White, A. B., J. R. Jordan, B. E. Martner, F. M. Ralph, and B. W. Bartram, 2000: Extending the dynamic range of an S-band radar for cloud and precipitation studies. *J. Atmos. Oceanic Technol.,* **17,** 1226–1234, doi:10.1175/1520-0426(2000)017<1226:ETDROA>2.0.CO;2.

——, P. J. Neiman, F. M. Ralph, D. E. Kingsmill, and P. O. G. Persson, 2003: Coastal orographic rainfall processes observed by radar during the California land-falling jets experiment. *J. Hydrometeor.,* **4,** 264–282, doi:10.1175/1525-7541(2003)4<264:CORPOB>2.0.CO;2.

Young, C. B., B. R. Nelson, A. A. Bradly, J. A. Smith, C. D. Peters-Lidard, A. Kruger, and M. L. Baeck, 1999: An evaluation of NEXRAD precipitation estimates in complex terrain. *J. Geophys. Res.,* **104** (D16), 19 691–19 703, doi:10.1029/1999JD900123.

Zhang, J., C. Langston, and K. Howard, 2008: Brightband identification based on vertical profiles of reflectivity from the WSR-88D. *J. Atmos. Oceanic Technol.,* **25,** 1859–1872, doi:10.1175/2008JTECHA1039.1.

——, Y. Qi, D. Kingsmill, and K. Howard, 2012: Radar-based quantitative precipitation estimation for the cool season in complex terrain: Case studies from the NOAA Hydrometeorology Testbed. *J. Hydrometeor.,* **13,** 1836–1854, doi:10.1175/JHM-D-11-0145.1.